Nitrous Acid Budgets in Coastal Atmosphere: Potential Daytime Marine Sources

Xuelian Zhong[1], Hengqing Shen[1*], Min Zhao[1], Ji Zhang[1], Yue Sun[1], Yuhong Liu[1], Yingnan Zhang[1], Ye Shan[1], Hongyong Li[1], Jiangshan Mu[1], Yu Yang[1], Yanqiu Nie[1], Jinghao Tang[2], Can Dong[1], Xinfeng Wang[1], Yujiao Zhu[1], Mingzhi Guo[2], Wenxing Wang[1], and Likun Xue[1*]

[1]Environment Research Institute, Shandong University, Qingdao, Shandong, 266237, China

[2]Collage of Mechanics and Materials, Hohai University, Nanjing, Jiangsu, 210098, China

Correspondence to Hengqing Shen (hqshen@sdu.edu.cn) and Likun Xue (xuelikun@sdu.edu.cn)

Abstract.

Nitrous acid (HONO), a vital precursor of atmospheric hydroxyl radicals (OH), has been extensively investigated to understand its characteristics and formation mechanisms. However, discerning fundamental mechanisms across diverse environments remains challenging. This study utilizes measurements from Mount Lao, a coastal mountain in eastern China, and an observation-based chemical box model (OBM) to examine HONO budgets and their subsequent impacts on atmospheric oxidizing capacity. The model incorporates additional HONO sources, including direct emissions, heterogeneous conversions of NO_2 on aerosol and ground surfaces, and particulate nitrate photolysis. The observed mean HONO concentration was 0.46 ± 0.37 ppbv. The updated model well reproduced daytime HONO concentrations during dust and photochemical pollution events. During dust events, daytime HONO formation was dominated by photo-enhanced heterogeneous reactions of NO_2 on aerosol surfaces (>50%), whereas particulate nitrate photolysis (34%) prevails during photochemical pollution events. Nevertheless, the model uncovers a significant unidentified marine HONO source in the "sea case", with its HONO production rate reaching up to 0.70 ppbv h^{-1} at noon. Without considering this unidentified source, an extraordinarily high photolysis coefficient of nitrate and/or heterogeneous uptake coefficient of NO_2 would be required to match observed HONO concentrations. This missing marine HONO source affected the peak O_3 production rate and OH radical concentration by 36% and 28%, respectively, at the observation site. Given the limited HONO observation data in coastal and marine settings, the unidentified HONO source may cause an underestimation of the atmosphere's oxidizing capacity. This study highlights the necessity for further investigation of the role of HONO in atmospheric chemistry in coastal and marine environments.

1 Introduction

Atmospheric nitrous acid (HONO) serves as a pivotal precursor of hydroxyl radicals (OH) (Alicke et al., 2003), accounting for up to 60% of daytime OH radicals (Kleffmann et al., 2005; Czader et al., 2012). Thus, HONO establishes itself as a critical source of OH radical source in both urban and rural environments, surpassing the contribution from ozone (O_3) photolysis (Acker et al., 2006; Elshorbany et al., 2012; Gu et al., 2022a). Consequently, HONO substantially influences the formation of secondary pollutants, including secondary aerosols and O_3, exerting a considerable effect on air quality and climate change (Xing et al., 2019; Yang et al., 2021b).

Recent studies pinpoint four primary sources of atmospheric HONO: (a) Direct emissions from traffic (Liao et al., 2021), biomass burning (Nie et al., 2015; Theys et al., 2020), soil (Su et al., 2011), and livestock farming (Zhang et al., 2023). (b) Homogeneous reaction of NO + OH, which is generally regarded as a significant process in polluted urban areas during daytime when NO and OH concentrations are relatively high (Gu et al., 2022a). (c) Heterogeneous reactions of NO_2 on various surfaces, such as mineral dust (Underwood et al., 2001), soil (Kebede et al., 2016), and aqueous surfaces (Wojtal et al., 2011). The uptake coefficient of NO_2, $\gamma(NO_2)$, on these surfaces remains uncertain and is subject to varying factors, sparking debates regarding the importance of the heterogeneous conversion of NO_2 (Broske et al., 2003; Xue et al., 2022). (d) Photolysis of adsorbed nitric acid (HNO_3) and particulate nitrate (pNO_3^-), crucial contributors to daytime HONO formation (Ye et al., 2017; Gen et al., 2022), particularly in clean environments (Zhou et al., 2011; Ye et al., 2016a). However, HONO formation mechanisms in different environments remain contentious and require more detailed model evaluations (Jiang et al., 2022).

Despite its short daytime atmospheric lifetime, HONO is frequently observed at high concentrations at noon (Ye et al., 2016a; Yang et al., 2021a; Jiang et al., 2023). Traditional mechanisms cannot fully explain these observed daytime HONO peaks, indicating the presence of additional daytime HONO sources (missing sources of daytime HONO). Over recent decades, researchers have extensively investigated the missing sources of daytime HONO in various environments (Kleffmann, 2007; Lee et al., 2016; Jiang et al., 2022; Zhang et al., 2022). However, our limited understanding of these unidentified HONO sources has hindered accurate assessments of atmospheric free radicals and oxidizing capacity (Tang et al., 2015). In areas with high concentrations of NO_2 and particulate matter, missing sources are often ascribed to the photolytic enhancement of heterogeneous NO_2 reactions (Su et al., 2008; Czader et al., 2012; Lee et al., 2016; Tong et al., 2016), which also can be intensified by the presence of other substances (e.g., ammonia or sulfur dioxide) (Ma et al., 2017; Li et al., 2018b; Ge et al., 2019). Conversely, in remote areas, nitrate photolysis or soil emissions are perceived as

significant contributors to daytime HONO sources (Su et al., 2011; Ye et al., 2016a; Cui et al., 2019). In polluted mountainous areas, the vertical transport of air masses may also contribute to observed daytime HONO concentrations (Jiang et al., 2020; Xue et al., 2022). During dust storms, the particle surface area increases sharply, potentially enhancing the heterogeneous reaction of NO_2, yet the evaluations of dust impacts on daytime HONO are scarce (Wang, 2003). Overall, most existing HONO source studies lack quantitative assessments based on models and fail to provide comparative analyses across different environmental scenarios.

The marine boundary layer (MBL) with a large air/water interface, where the ocean and atmosphere exchange trace gases, heat, and aerosol particles (Wurl et al., 2016), and the interfacial photochemistry processes often occur (Bruggemann et al., 2018), is utterly different from inland environments. The opposite diurnal variations of HONO with a peak concentration at noon at marine sites implied the different predominant HONO processes compared with polluted inland areas (Jiang et al., 2022). Furthermore, recent observations of HONO in coastal and marine regions indicate the existence of marine HONO sources (Ye et al., 2016a; Crilley et al., 2021; Yang et al., 2021a; Jiang et al., 2022). The observed accelerated NO_2-to-HONO conversion in marine air masses suggests that air-marine interactions enhance HONO production (Zha et al., 2014; Yang et al., 2021a). However, the heterogeneous conversion of NO_2 on vast air/water interface, a potential source of marine HONO, remains uncertain (Wojtal et al., 2011; Yu et al., 2021; Zhu et al., 2022). Crilley et al. (2021) only obtained a factor of 5 lower ocean-surface NO_2-to-HONO conversion than previous studies; there was still a debate on the importance of ocean-surface-mediated conversion of NO_2 into HONO. Nitrate photolysis is believed to contribute to marine HONO sources (Ye et al., 2016a; Andersen et al., 2023), but significant controversy persists (Romer et al., 2018; Shi et al., 2021). The specific influencing factors remain unclear (Zhang et al., 2020; Andersen et al., 2023), with some studies suggesting other factors may be responsible (Wojtal et al., 2011; Yang et al., 2021a). Accordingly, Jiang et al. (2023) highlighted the contribution of the dust-surface-photocatalytic conversion of reactive nitrogen compounds to HONO formation and the important role of halogen chemistry in HONO simulation in CVAO. However, most existing studies still rely on steady-state analysis, and there is a lack of quantitative research determining if current HONO mechanisms can adequately explain observed marine daytime HONO concentrations.

Mount Lao, located on the eastern coast of Qingdao, China, experiences influences from various air masses from the continent and the ocean. During the spring of 2021 (27 April–19 May), when dust and O_3 pollution occurred frequently, we conducted measurements on Mount Lao to explore the daytime HONO budgets in the coastal atmosphere. Utilizing the latest HONO formation mechanisms

97   in the box model, we found that the existing parameters adequately accounted for the HONO sources

98   during both dust and photochemical pollution periods. However, we identified a significant

99   discrepancy between the simulated and observed HONO in the "sea case". This discrepancy suggests

100 that a substantial daytime source of marine-derived HONO is absent from the current chemical

101 mechanisms. To compensate for this missing source, either an unprecedentedly large enhancement

102 factor (EF) of nitrate photolysis or a heterogeneous uptake coefficient of NO_2 would be necessary if

103 attributed solely to these known HONO sources.

2 Methods

2.1 Field measurements

106   Field measurements were conducted on the southeast coast of Mount Lao (36.15°N, 120.68°E,

107 166 m above sea level) in Qingdao (Figure 1), approximately 1 km away from the Yellow Sea. The

108 geographical location and elevation of Mount Lao make it an optimal location for examining the

109 contrasts between marine and continental air masses and the chemical processes within the marine

110 boundary layer. The relatively pristine condition of the area, coupled with minimal levels of

111 anthropogenic activities such as industrial emissions, establish Mount Lao as a representative of a

112 clean environment. The field campaign was carried out during the spring of 2021 (27 April–19 May

113 2021), a period when the air quality of Qingdao is often affected by dust storms from Mongolia and

114 northwestern China, as well as by O_3 pollution. Consequently, the site at Mount Lao provides an

115 opportune platform for investigating the fundamental formation mechanisms of HONO under diverse

116 environmental conditions.

117   HONO was quantified using a water-based long-path absorption photometer (WLPAP, Beijing

118 Zhichen Technology Co., Ltd, China). Ambient HONO was absorbed by deionized water alone, after

119 which it reacted with a reagent comprising 3.44 g of sulfanilamide and 0.2 g of N-(1-naphthyl)-

120 ethylenediamine-dihydrochloride (NED) in 10 liters of deionized water, leading to the formation of an

121 azo dye. Two channels were employed to extract HONO and interfering gases, respectively. The

122 absorbance of the azo dye was measured using a fiber optic spectrometer (USB 4000, Ocean Optics,

123 USA) at both the measurement wavelength (550 nm) and the reference wavelength (580 nm). Regular

124 automatic zero measurements using ultrapure nitrogen were conducted every two days to correct for

125 baseline drift. The detection limit and detection ranges were 2 pptv and 5 pptv–2 ppmv, respectively.

126   A suite of commercial online analyzers monitored the concentrations of NO_x, O_3, SO_2, and CO

127 (42i, 49i, 43i, and 48i, respectively, Thermo Fisher Scientific Inc, USA). $PM_{2.5}$ was measured using a

128 hybrid nephelometric/radiometric particulate mass monitor (SHARP-5030i, Thermo Fisher Scientific

Inc, USA), while PM_{10} mass data were obtained from the China National Environmental Monitoring Center (https://quotsoft.net/air/). During the field campaign, fifty-seven VOC (volatile organic compound) canister samples were collected at 2-hour intervals from 9:00–19:00 local time on pollution episode days and at 6-hour intervals from 9:00–21:00 on non-episode days. These VOC samples were subsequently analyzed using gas chromatography and mass spectrometry (TT24xr, Markes, UK; GC–MS, Thermo Fisher Scientific Inc, USA) (Liu et al., 2021). A wide-range particle spectrometer (WPS, Model 1000XP, MSP, USA) was employed to determine the atmospheric particle number size distributions from 10 nm to 10 μm. Taking into account the hygroscopic growth, the relative humidity-adjusted aerosol surface area concentration (Sa) was calculated based on the determined particle number size distributions. 95 offline particulate samples were collected every 3-hour interval from 7:00–19:00 and 12-hour intervals from 19:00–7:00 utilizing a high-volume air-sampling system (TE-5170, Tisch Environmental Inc, USA). The inorganic compositions of the samples, including Cl^-, NO_3^-, SO_4^-, NH_4^+, Na^+, K^+, Mg^{2+}, and Ca^{2+}, were determined via ion chromatography (Dionex ICS-600, Thermo Fisher Scientific Inc, USA). Meteorological data, including temperature, RH, pressure, wind speed, and wind direction, were monitored by an ultrasonic integrated weather station (RS-FSXCS-N01-1).

This study distinguishes between the "sea case" and the "land case" by analyzing the backward trajectory of the air mass. Specifically, considering the short lifetime of HONO, the MeteoInfo model (Wang, 2012) was used to calculate 6-hour air mass backward trajectories starting at the height of 200 meters above ground level, using meteorological parameters from the Global Data Assimilation System (GDAS, ftp://arlftp.arlhq.noaa.gov/). The criteria for differentiating between the "sea case" and "land case" is based on the time spent over land or sea during the 6-hour backward air mass, with cases that spent less than 1 hour over land designated as a "sea case" (Yang et al., 2021a). Following this criterion, we selected a total of 18 sea cases and 13 land cases (Table S1). The observation data for the "sea case" and the "land case" were averaged for subsequent analysis.

2.2 Model setup

An observation-based chemical box model (OBM) was employed to explore the HONO budgets and atmospheric oxidizing capacity. The chemical mechanism used for the modeling was obtained from the Master Chemical Mechanism (MCM) website (http://mcm.york.ac.uk/) and was based on the MCM v3.3.1 as proposed by Jenkin et al. (2015). The model was constrained with data including HONO, O_3, NO, NO_2, SO_2, CO, VOCs, pNO_3^-, Sa, temperature, RH, pressure, and JNO_2. The observed data of HONO, O_3, NO, NO_2, SO_2, CO, VOCs, pNO_3^-, Sa, temperature, RH, and pressure were averaged or interpolated to a time resolution of 5 minutes, except for VOCs and pNO_3^-, which

162 were linearly interpolated to a time resolution of 1 hour to constrain the model (Yang et al., 2018). The

163 calculation of the photolysis rate of NO$_2$, JNO$_2$, was determined using Equation 1:

$$JNO_2 = JNO_{2(TUV)} \times \frac{UV_{observed}}{UV_{TUV}}$$ (E1)

164 where JNO$_{2(TUV)}$ and UV$_{TUV}$ are obtained from the Tropospheric Ultraviolet and Visible (TUV)

165 radiation model (http://cprm.acom.ucar.edu/Models/TUV/Interactive_TUV/). The UV$_{observed}$ was

166 obtained from the NASA GES DISC (https://disc.gsfc.nasa.gov/). Other photolysis frequencies were

167 calculated in the OBM and scaled by JNO$_2$. The time series of JNO$_2$ is presented in Figure S1. The

168 model was pre-run for 1 day to stabilize the simulation of unconstrained species.

169   In the MCM v3.3.1, the formation of HONO is originally attributed to a homogeneous reaction,

170 specifically NO + OH → HONO. This study extends the existing mechanism by incorporating

171 additional sources of HONO into the chemical model. A description of these sources and their

172 associated mechanisms is provided in the following, and the corresponding parameters are listed in

173 Table 1.

Description of HONO sources and sinks adopted in the OBM

Direct emission

176 In the atmosphere, HONO can be directly released through the exhaust emissions of various sources.

177 The HONO/NO$_x$ emission ratio, which typically averages around 0.8%, is a common parameter used

178 to gauge the impact of these vehicular emissions on HONO concentration (Kleffmann et al., 2003;

179 Czader et al., 2012; Lee et al., 2016; Xue et al., 2020a). However, the ratio can fluctuate between 0.3%

180 and 1.6%, depending on engine and fuel types (Kurtenbach et al., 2001). Prior research indicates that

181 direct emissions contribute significantly to HONO concentration in urban settings (Zhang et al., 2019;

182 Kramer et al., 2020). However, in rural and background areas, the vehicular contribution is

183 comparatively insignificant (Liu et al., 2019b; Xue et al., 2022). Consequently, the contribution of

184 vehicle emissions to HONO is not constant and varies based on the environment and traffic density.

185 In this study, we employed the widely used ratio of 0.8% for modeling scenarios and sensitivity

186 simulations using ratios of 0.4% and 1.6%.

Homogeneous reaction of OH + NO → HONO

   NO + OH + M → HONO + M (R1)

188 The reaction of NO + OH is considered an important gas-phase reaction for HONO formation,

189 particularly during pollution periods when concentrations of NO and OH are high (Gu et al., 2022a).

190 We employed the box model to calculate the reaction rate using complex rate coefficients from the

191 MCM website (http://mcm.york.ac.uk/parameters/complex.htt).

Heterogeneous reaction of NO$_2$ on aerosol surfaces

$$NO_2 + H_2O \xrightarrow{\text{aerosol surface}} HONO + HNO_3 \tag{R2}$$

$$NO_2 + hv \xrightarrow{\text{aerosol surface}} HONO \tag{R3}$$

$$k_{aerosol} = 0.25 \times v_{NO_2} \times S_a \times \gamma_a \qquad \gamma_a = 8 \times 10^{-6} \tag{E2}$$

$$k_{aerosol,\,hv} = 0.25 \times v_{NO_2} \times S_a \times \gamma_{a,\,hv} \times \frac{JNO_2}{JNO_{2,noon}} \qquad \gamma_{a,\,hv} = 4 \times 10^{-5} \tag{E3}$$

$$v_{NO_2} = \sqrt{\frac{8RT}{\pi M}} \tag{E4}$$

193 The heterogeneous conversion of NO$_2$ on surfaces is a significant source of HONO in the atmosphere.

194 As illustrated by equations R2 and R3, NO$_2$ reacts with water and light on aerosol surfaces to produce

195 HONO. The HONO formation rate from heterogeneous reactions is typically first-order with respect

196 to NO$_2$ concentration (Aumont et al., 2003), and the reactivity of NO$_2$ is known to be significantly

197 enhanced under irradiated conditions compared to darkness (Yu et al., 2022a). In this study, the uptake

198 coefficients of NO$_2$ on the aerosol surface in dark and irradiated conditions, γ_a and $\gamma_{a,\,hv}$, were set to

199 8×10^{-6} and 4×10^{-5} (Lelièvre et al., 2004; Vandenboer et al., 2013), respectively. The molecular speed

200 of NO$_2$ (v_{NO_2}, m s^{-1}) was calculated using Equation 4, where R represents the ideal gas constant, 8.314

201 J mol^{-1} k^{-1}, T is the absolute temperature (K), and M is the relative molecular weight of NO$_2$ (g mol$^-$

202 ^{1}). Sa is the surface area concentration (m^2 m^{-3}) estimated from particle number concentrations

203 measured by the WPS.

Heterogeneous reaction of NO$_2$ on ground surfaces

$$NO_2 + H_2O \xrightarrow{\text{ground surface}} HONO + HNO_3 \tag{R4}$$

$$NO_2 + hv \xrightarrow{\text{ground surface}} HONO \tag{R5}$$

$$k_{ground} = 0.25 \times v_{NO_2} \times \gamma_{g,\,hv} \times \frac{S}{V} \qquad \gamma_g = 1 \times 10^{-6} \tag{E5}$$

$$k_{ground,\,hv} = 0.25 \times v_{NO_2} \times \gamma_{g,\,hv} \times \frac{S}{V} \times \frac{JNO_2}{JNO_{2,noon}} \qquad \gamma_{g,\,hv} = 2 \times 10^{-5} \tag{E6}$$

$$\frac{S}{V} = \frac{1.7}{BLH} \tag{E7}$$

205 Equations 5 and 6 delineate the parameterizations for the heterogeneous reaction of NO$_2$ on the ground

206 surfaces, both in the absence and presence of light. The uptake coefficients of NO$_2$ on the ground

207 surface under dark and irradiated conditions, γ_g and $\gamma_{g,\,hv}$, respectively, were set to 1×10^{-6} and 2×10^{-5}

208 (Kleffmann et al., 1998; Stemmler et al., 2006), respectively. Under ambient conditions, the relative

importance of gas uptake on ground and aerosol surfaces is uncertain, with the influence of land use categories and chemical compositions (Li et al., 2019). The surface-to-volume ratio, $\frac{S}{V}$, is calculated by an effective surface of 1.7 m^2 per geometric surface in Equation 7 (Vogel et al., 2003). Within the model, the boundary layer height, BLH, is projected to increase from 300 m at dawn to 1500 m at 14:00 and then decrease back to 300 m at dusk (Xue et al., 2014).

Photolysis of particulate nitrate

$$pNO_3^- + h\nu \rightarrow HONO \tag{R6}$$

$$k = \frac{J(pNO_3^-)}{JHNO_{3,noon}} \times JHNO_{3(MCM)} \tag{E8}$$

In Equation 8, the photolysis rate constant of gaseous HNO$_3$ at noon, JHNO$_{3,noon}$, is chosen to be $\sim 7 \times 10^{-7}$ s^{-1} based on previous studies (Ye et al., 2016b). JHNO$_{3(MCM)}$ is calculated by the box model. Recent research has shown that the photolysis rate of particulate nitrate is significantly faster than that in the gas and aqueous phases (Zhou et al., 2003; Ye et al., 2016a). We adopt a median value of 8.3×10^{-5} s^{-1} in our simulation based on a range provided by Ye et al. (2017). Considering the uncertainty of the parameter values of the above-mentioned HONO formation mechanisms, we conducted the sensitivity tests with lower and upper values in Sections 3.2 and 3.3.

Photolysis of HONO

$$HONO + h\nu \rightarrow OH + NO \tag{R7}$$

The primary loss pathway of HONO is through photolysis following sunrise, which significantly contributes to the atmospheric OH budget. The photolysis rate of HONO, J(HONO), in the OBM, is constrained by JNO$_2$.

Homogeneous reaction between HONO and OH

$$HONO + OH \rightarrow H_2O + NO_2 \tag{R8}$$

The relevant kinetic parameter of the reaction between HONO and OH is available from the MCM mechanism, and its reaction rate coefficient is dependent solely on the temperature.

Dry deposition of HONO

$$k = \frac{v_{HONO}}{BLH} \tag{E9}$$

Here, v_{HONO} is the dry deposition velocity of HONO (cm s^{-1}). Harrison and Kitto (1994) suggested the range of v_{HONO} was 0.2–1.7 cm s^{-1}, and a value of 1.0 cm s^{-1} was employed in this study. The dry deposition of HONO, ozone, and other species, including peroxides, carbonyls, and organic acids, are also considered in the OBM model (Xue et al., 2014).

3 Results and discussion

3.1 Concentration levels and temporal variations

Figure 2 displays the time series of HONO, $HONO/NO_2$, NO_x, O_3, CO, SO_2, $PM_{2.5}$, and pNO_3^-, along with meteorological parameters (i.e., temperature, RH, and wind) measured throughout the field campaign. The presence of missing data in the time series resulted from instrument maintenance and calibration. Instrument maintenance and calibration resulted in gaps in the time series data. The observation site underwent dust periods on April 27–28 and May 7–8, as well as periods of photochemical pollution on May 5–6, 13, and 17–18. In this study, a photochemical pollution period is classified as a day when the maximum daily 8-hour average O_3 concentration ($MDA8O_3$) exceeds 75 ppbv (the Grade II National Ambient Air Quality Standard). A dust period is recognized when the peak PM_{10} concentration surpasses 150 µg m^{-3}, and the $PM_{2.5}/PM_{10}$ ratio falls below 0.4, based on previous research (Liu et al., 2006; Wu et al., 2020). Section 3.2 provides a comprehensive explanation of the differences in pollutant concentrations and HONO budgets during dust and photochemical pollution periods.

Table 2 summarizes the descriptive statistics of the species and meteorological parameters measured during the observation period. The average (± standard deviation, SD) temperature and RH were 15.1 ± 3.4 °C and $68.7 \pm 26.1\%$, respectively, indicating a moderate spring temperature and relatively high RH influenced by marine air masses. The primary pollutant concentrations were relatively low, as indicated by the mean mixing ratios of 0.9 ± 1.7 ppbv, 5.9 ± 4.8 ppbv, 284.0 ± 118.8 ppbv, and 1.0 ± 0.8 ppbv for NO, NO_2, CO, and SO_2, respectively. These low levels suggest Mount Lao is a relatively clean site with minimal impact from nearby anthropogenic sources. The high O_3 concentration (60.4 ± 15.8 ppbv) implies that photochemical reactions were relatively strong during observation. The mean concentrations of $PM_{2.5}$ and pNO_3^- were 21.2 ± 21.09 µg m^{-3} and 4.6 ± 5.0 µg m^{-3}, respectively.

During the campaign, the mean concentration of HONO was 0.46 ± 0.37 ppbv, with a maximum mixing ratio of 3.14 ppbv recorded at 17:00 on May 4th. The concentration level of HONO at Mount Lao is lower than at urban sites with higher NO_2 concentrations (Li et al., 2018a; Hao et al., 2020; Yu et al., 2022b). However, it is notably higher than other clean coastal and remote marine sites, as Table S2 illustrates (Villena et al., 2011; Zha et al., 2014; Meusel et al., 2016; Crilley et al., 2021; Zhu et al., 2022). Past research conducted in urban and rural areas found that the $HONO/NO_2$ ratio, which indicates the extent of NO_2 conversion to HONO, typically ranges from 0.02 to 0.08 (Jiang et al., 2022).

265 The higher HONO/NO₂ value (0.13) measured at Mount Lao highlights the potentially significant role
266 of non-NO$_x$ related HONO sources or higher heterogeneous conversion of NO₂ efficiency at this site.

267   Figure 3 illustrates the average diurnal patterns of HONO and related species. The diurnal cycle
268 of CO and SO₂ is similar, with peak concentrations observed during midday and relatively stable
269 concentrations during nighttime. The concentration of O₃ increases with the accumulation of
270 photochemical generation during the afternoon and decreases steadily after sunset. Contrary to most
271 urban or rural locations, the concentration of HONO at Mount Lao peaks at noon, similar to remote
272 areas (Ye et al., 2016a; Jiang et al., 2022). It is important to note that both HONO and NO$_x$ exhibit a
273 second daytime peak in the late afternoon, primarily caused by specific days with relatively high
274 emissions or transport events. After excluding these days, the diurnal variation of HONO aligns more
275 closely with observations in clean regions (Jiang et al., 2022). We have included the diurnal variation
276 of HONO after removing days with afternoon peaks in the supporting information. Since their impact
277 is largely confined to specific days, it does not significantly affect our subsequent analysis, particularly
278 the "sea case" analysis. NO$_x$, comprising NO and NO₂, shows a similar temporal variation trend to
279 HONO, suggesting potential photolytic sources for them (Reed et al., 2017). During the daytime (7:00–
280 17:00), the average concentration of HONO was 1.56 times higher than at night (17:00–7:00), with
281 concentrations of 0.54 ppbv during the day and 0.35 ppbv at night. Given the short lifetime of HONO
282 during the day—only a matter of minutes—the noon HONO peak concentration suggests an in situ
283 photochemical source for HONO (Kasibhatla et al., 2018). The ratio of HONO to NO₂ shows an
284 increasing trend until sunrise, suggesting heterogeneous conversion from NO₂ to HONO during
285 nighttime. However, unlike urban areas where the ratio of HONO to NO₂ decreases during the daytime
286 (Zhang et al., 2019; Gu et al., 2022a), the ratio even increases during the midday period at Mount Lao,
287 implying that HONO from sources other than NO₂ conversion also significantly contributes to HONO
288 concentration (Yang et al., 2021a). Considering that the influence of HONO on the OH radical and O₃
289 is primarily observed during the daytime, the higher concentration of HONO during the daytime at the
290 Mount Lao site suggests the presence of strong daytime HONO sources. The primary objective of our
291 following study is to analyze the daytime budgets of HONO in the coastal atmosphere of Mount Lao.

3.2 Daytime HONO budgets in dust and photochemical pollution periods

293   The daytime HONO budgets were examined during periods of dust and photochemical pollution
294 using an updated OBM, with the aim of assessing whether our current understanding of HONO sources
295 is sufficient to explain observed concentrations. Table 4 presents the mean daytime concentrations of
296 HONO and other species during the dust, photochemical pollution, and non-polluted periods (i.e., days
297 devoid of dust and photochemical pollution). On average, the daytime HONO concentrations during

dust and photochemical pollution periods were 0.57 ± 0.39 ppbv and 0.44 ± 0.29 ppbv, respectively. The dust period exhibited significantly higher concentrations of NO_2, $PM_{2.5}$, pNO_3^-, and Sa, with increased factors of 1.4, 2.6, 2.3, and 2.3, respectively, compared to the non-polluted period. During the photochemical pollution period, the daytime mean values of O_3, CO, SO_2, $PM_{2.5}$, pNO_3^-, and JNO_2 were 78.8 ppbv, 353.8 ppbv, 1.7 ppbv, 25.0 μg m^{-3}, 6.2 μg m^{-3}, and 7.0×10^{-3} s^{-1}, respectively. These values were approximately 1.4, 1.3, 2.4, 1.5, 2.1, and 1.6 times higher than those during the non-polluted period.

Figure 4 compares the observed and modeled HONO concentrations during dust and photochemical pollution periods and illustrates the contribution of various sources and sinks to the HONO budget. The study examined two scenarios: the base case, which only considered the homogeneous reaction NO + OH, and the model case, which considered all seven HONO sources outlined in Table 1. The results indicated that the base case significantly underestimated the HONO concentration, consistent with previous studies (Liu et al., 2019b; Zhu et al., 2022). However, the model case effectively replicated the observed HONO concentrations for both periods, even the high noon concentrations. The index of agreement (IOA) values for HONO during the dust and photochemical pollution periods were 0.96 and 0.88, respectively. This suggests that the updated parameterization scheme employed in the model can adequately account for the observed HONO concentrations at Mount Lao.

During the daytime, the average modeled production rates of HONO were 1.66 ppbv h^{-1} and 0.90 ppbv h^{-1} for the dust and photochemical pollution periods, respectively. The maximum HONO production rate was significantly higher during the dust period (3.50 ppbv h^{-1}) compared to the photochemical pollution period (1.69 ppbv h^{-1}) and was even comparable to levels observed during haze periods at polluted urban or rural sites (Zhang et al., 2019; Xue et al., 2020b; Gu et al., 2022a). Based on the model results of detailed HONO budgets, the dominant pathway for daytime HONO production during the dust period was photo-enhanced heterogeneous conversion of NO_2 on the aerosol surface, accounting for 53% (0.87 ± 0.66 ppbv h^{-1}) of the simulated daytime HONO production rate. Wang (2003) reported sudden increases in HONO concentration during nocturnal dust storm events and observed a higher ratio of HONO to NO_2 (0.18). The enhanced efficiency of NO_2 to HONO on mineral dust particles suggests a potentially significant impact of dust aerosol on nitrogen compound distribution. Further research is needed to understand the contribution of dust to HONO formation and nitrogen cycling during the daytime, as well as its global impact. For the photochemical pollution period, the major sources of HONO included the photolysis of particulate nitrate, the photo-enhanced heterogeneous conversion of NO_2 on the aerosol surface, and the homogeneous reaction of

OH and NO, which contributed 34%, 27%, and 27% of the daytime HONO production rate, respectively. This points to the significant role of photochemical processes under intense solar radiation. Direct emissions had a negligible contribution during both the dust and photochemical pollution periods, accounting for less than 2%. The photolysis of HONO was the dominant loss pathway throughout the day for all measurement periods, accounting for more than 90% of HONO sinks.

The model was subjected to sensitivity tests by increasing or decreasing selected parameters by factors of 5 and 2 (Table S4, Figures S3, and S4). Even with such a broad range of parameter variation, the heterogeneous reaction of NO_2 on aerosols and the photolysis of nitrate to form atmospheric HONO remained significant sources of HONO under both dust and photochemical pollution periods. This suggests that our current understanding of HONO sources, based on existing mechanisms, can generally explain the observed concentrations of HONO. However, it is important to note that differences in parameter selection can significantly affect the relative contributions of each pathway. Given the considerable uncertainties in the uptake coefficient of NO_2 and the enhancement factors of photolysis of nitrate, further experimental studies are necessary to evaluate their effects on HONO in different environmental conditions.

3.3 Missing daytime HONO source in "sea case"

Recent field studies suggest potential unidentified daytime sources of nitrous acid (HONO) in the marine atmosphere, with high daytime HONO levels recorded (Ye et al., 2016a; Yang et al., 2021a). Figure 5 shows the diurnal variation of the selected "sea case" and "land case", with corresponding statistical results in Table S3. In the "sea case", daytime concentrations of typical primary pollutants, such as CO and SO_2, are significantly lower than those in the "land case" (251 ± 59 ppbv vs. 335 ± 115 ppbv and 0.7 ± 0.4 ppbv vs. 1.4 ± 0.8 ppbv for CO and SO_2, respectively). Concurrently, the "sea case" shows a lower daytime temperature (15.2 ± 3.0℃ vs. 18.7 ± 3.8℃) and higher RH (76.3 ± 25.9% vs. 47.3 ± 20.3%) compared to the "land case". This is consistent with our understanding of marine air masses, which tend to be cleaner and more humid. These findings validate our classification method of "land case" and "sea case" based on the backward air mass trajectory.

Secondary pollutants in marine air masses, such as O_3, $PM_{2.5}$, and pNO_3^-, also register lower daytime concentrations than in the "land case" (59.4 ± 10.3 ppbv vs. 63.4 ± 13.3 ppbv, 13.2 ± 5.8 μg m^{-3} vs. 29.9 ± 22.8 μg m^{-3}, and 1.3 ± 0.5 μg m^{-3} vs. 10.0 ± 3.3 μg m^{-3}, respectively). Though the HONO concentration in marine air masses is less than that in the "land case" (0.42 ± 0.25 ppbv vs. 0.51 ± 0.22 ppbv), it maintains a relatively high level, particularly during intense photolysis periods around noon when the HONO concentration in the "sea case" marginally increases. NO_x

concentrations in the "sea case" are also lower than in the "land case", but the difference is less substantial than primary pollutants, with both NO and NO_2 showing concentration peaks around noon. Nighttime observations in the "sea case" show a higher $HONO/NO_2$ ratio (0.12), which has been noted in earlier studies (Zha et al., 2014), suggesting strong nocturnal HONO formation in marine air masses. Here, we focus on the sources of HONO during the day under the influence of marine air masses.

Utilizing the updated chemical model, we examine the HONO budgets in both "sea" and "land" cases. In the "land case", the simulated HONO concentration aligns well with the observed HONO concentration, with a high index of agreement (IOA) value of 0.94 (Figure 6a). The peak HONO production rate observed at Mount Lao (2.69 ppbv h^{-1}) surpasses that calculated in continental air masses at Hok Tsui, Hong Kong (less than 1.5 ppbv h^{-1}) (Gu et al., 2022b). The contributions of photo-enhanced heterogeneous reactions of NO_2 on the aerosol surface (22%) and photolysis of pNO_3^- (20%) are comparable (Figure 6c). Model results reveal that the homogeneous reaction between NO and OH is the predominant HONO formation pathway, contributing an average of 44% (0.52 ± 0.38 ppbv h^{-1}). Despite a lower absolute rate than in urban areas, the relative contribution is significant(Gu et al., 2022a; Yu et al., 2022b). This result suggests that similar to the findings in the cases of dust and photochemical pollution, the current model's parameterization reasonably accounts for the observed HONO concentration in the "land case".

However, in the "sea case", while the updated model has improved in simulating HONO concentrations, with an average concentration increase from 0.05 ppbv to 0.11 ppbv, it falls short of the observed concentration (0.42 ppbv), indicating a substantial unidentified HONO source. At noon, the missing HONO production rate ($P_{missing}$) can reach up to 0.70 ppbv h^{-1}. This value is slightly higher than the result calculated by Meusel et al. (2016) on Cyprus Island (about 0.5 ppbv h^{-1}), but lower than that reported by Yang et al. (2021a) in coastal Qingdao (up to 1.83 ppbv h^{-1}, including all non-NO+OH pathways). Sensitivity tests were conducted to assess the impact of parameter selection on simulation results, but even with much larger parameters (Table S4), the model fails to explain the observed HONO concentrations (Figure S5).

The correlation analysis reveals that the missing HONO production rate correlates strongly with JNO_2 and $JNO_2 \times pNO_3^-$ (Figure S7), with correlation coefficients (r) of 0.90 and 0.73, respectively. This indicates that the missing HONO sources are closely related to photochemical processes. This concurs with recent multi-site HONO analysis results, which propose a significant role of photochemical processes in observed HONO concentrations in remote areas (Jiang et al., 2022). We postulate that all missing HONO originates from photochemical processes and have calculated the required enhancement factors (EF) for nitrate photolysis rates (Text S2) and the uptake coefficient

required for NO_2 on aerosol and ground surfaces (Figure S6). To account for the observed HONO concentrations, the required EF is approximately 4000. While Andersen et al. (2023) noted that the EF increases with decreasing nitrate concentration, a 4000-fold difference exceeds all laboratory and field observations to date (Ye et al., 2017; Andersen et al., 2023). The required uptake coefficient of NO_2 on aerosol and ground surface reaches 4×10^{-4}, exceeding previous laboratory studies (Stemmler et al., 2007; Liu et al., 2019a). Although NO_2 uptake coefficients on the order of 10^{-4} have been measured in laboratory experiments under conditions of high SO_2 concentration (280 ppbv) and moderate acidity (pH = 5) (Liu and Abbatt, 2021), our observational site features lower SO_2 concentrations (~ 1ppbv) and slightly acidic aerosols (pH = 3.1). These conditions suggest that the uptake coefficients should be considerably lower than the laboratory-measured 2×10^{-4}. It is worth noting that previous research has indicated that the presence of halogens can enhance NO_2 uptake, which could potentially explain the higher NO_2 to HONO conversion ratios in marine environments (Yabushita et al., 2009). However, further research is needed to explore this possibility. Overall, the observed missing HONO source in the "sea case" cannot be explained by the current photochemical processes. This deviates from the findings of Zhu et al. (2022), who discovered that nitrate photolysis could explain the observed HONO concentrations in clean marine air masses using a moderate EF of 29. In recent years, many observations have noted distinct HONO characteristics under the influence of marine air masses, differing from those in continental air masses, but the specific mechanisms are still lacking (Meusel et al., 2016; Crilley et al., 2021; Yang et al., 2021a; Zhu et al., 2022). The ocean surface contains abundant nitrogen-containing substances (e.g., dissolved nitrate, ammonia, aliphatic amine, dissolved free amino acids) (Donaldson and George, 2012; Altieri et al., 2016), encompassing both organic and inorganic nitrogen. This is particularly true in polluted coastal areas where surface nitrogen content is rich. It merits investigation whether these nitrogen-containing substances in the alkaline sea-surface microlayer can directly affect HONO production or enhance HONO formation by photolysis on the formed sea salt aerosols. Additionally, the presence of halogens in oceanic air masses might promote nitrate photolysis (Zhang et al., 2020).

3.4 Impacts of HONO on O_3 and OH production

To quantify the impact of HONO, especially in the marine atmosphere, on O_3 and OH radicals, we conducted further scenario simulations using a chemical box model. In the "with HONO" scenario, we input the observed HONO concentrations to constrain the model. In contrast, in the "without HONO" scenario, we turn off seven HONO production pathways summarized in Table 1 and set the input HONO concentrations to zero. The differences between these scenarios illustrate the impact of HONO chemistry on O_3 and OH radicals in the atmosphere. To further investigate the effect of the

missing HONO sources in marine air masses, we established a third simulation scenario, "without

missing HONO", in the marine air mass simulation. In this scenario, the model includes the latest

HONO formation mechanisms discussed earlier but without the constraint of observed HONO.

HONO significantly influences the production of O_3 and OH radicals, regardless of whether the

overall situation during the observation period ("overall case") or the situation within the marine air

masses ("sea case") is considered (Figure 7). The net O_3 production rate is determined by the difference

between the O_3 production rate (P(O_3)) and loss rate (L(O_3)) (Xue et al., 2014). Specifically, the

absence of HONO resulted in a decrease in the net O_3 production rate and OH radical primary

production rate in the "overall case" from 7.39 ppbv h^{-1} and 1.44×10^7 molecules cm^{-3} s^{-1} to 3.41 ppbv

h^{-1} (a 54% reduction) and 2.81×10^6 molecules cm^{-3} s^{-1} (an 81% reduction), respectively. Regarding

concentration, the absence of HONO chemistry resulted in a reduction in the average OH radical

concentration from 3.6×10^6 molecules cm^{-3} to 1.9×10^6 molecules cm^{-3}, and the peak OH concentration

from 5.2×10^6 molecules cm^{-3} to 2.7×10^6 molecules cm^{-3}. Similarly, in the marine air masses, the

production rates of O_3 and OH decreased from 6.22 ppbv h^{-1} and 7.69×10^6 molecules cm^{-3} s^{-1} to 3.33

ppbv h^{-1} (a 46% reduction) and 2.14×10^6 molecules cm^{-3} s^{-1} (a 72% reduction), respectively without

HONO chemistry. These findings are consistent with previous observational studies (Yang et al.,

2021a; Gu et al., 2022a), highlighting the significant impact of HONO on O_3 and OH radicals in the

atmosphere.

Notably, in the "sea case", if the observed values are not input as constraints, and only the updated

mechanisms are used ("without missing HONO"), the model still significantly underestimates the

impact of HONO on O_3 and OH radicals. Specifically, missing marine HONO sources contributed 36%

to the peak net O_3 production rate(from 9.24 ppbv h^{-1} to 5.90 ppbv h^{-1})and 28% to peak OH

concentration (from 3.4×10^6 molecules cm^{-3} to 2.4×10^6 molecules cm^{-3}). Regarding the relative

contribution to OH radicals, HONO accounts for 79% and 55% in the "overall case" and "sea case",

respectively, both exceeding the combined contribution of other pathways (photolysis of O_3

contributes 14% and 25%, respectively). Given the relatively limited observational data on HONO in

coastal or marine areas and the unclear understanding of the missing HONO sources in the ocean, the

impact of marine emissions on atmospheric oxidizing capacity may be significantly underestimated.

This underscores the importance of further research in this area to enhance our understanding of the

role of HONO in atmospheric chemistry, especially in marine environments.

4 Conclusions

This study presents a comprehensive investigation of the characteristics and sources of nitrous

acid (HONO) in the coastal environment of Qingdao. The analysis utilizes observational data from the

Mount Lao site in Qingdao during spring 2021 and an updated chemical box model that integrates HONO mechanisms. The focus lies on discerning the unidentified HONO sources in marine air masses and comprehending their effects on atmospheric chemistry, emphasizing O_3 and OH concentrations.

Despite a relatively pristine coastal atmosphere, HONO concentrations are considerably higher than previously thought (0.46 ± 0.37 ppbv), notably during daytime. This observation persists in lower primary pollutant concentrations such as CO and SO_2 within marine air masses, suggesting missing HONO sources tied to photochemical processes. An updated chemical model's simulation reveals that the mechanisms behind HONO formation can satisfactorily account for the observed HONO concentrations during the dust and photochemical pollution periods. Yet, in marine scenarios, the model falls short of matching observed concentrations, pointing to a strong unidentified HONO source within the marine atmosphere. Sensitivity tests and correlation analyses emphasize the importance of photochemical processes in unidentified HONO sources. Nevertheless, if these unknown sources are attributed to either nitrate photolysis or heterogeneous NO_2 reactions, the necessary nitrate photolysis rate and the heterogeneous uptake coefficient of NO_2 would surpass the upper thresholds established by current laboratory studies. In light of these findings, future research must target uncovering the mechanisms behind the missing HONO sources in marine air masses. Specifically, the role of nitrogen-containing substances at the ocean's surface and the potential influence of halogens in promoting nitrate photolysis warrant further examination.

Acknowledgments

This work was supported by the National Science Foundation of China (grants nos. 42061160478 and 42105106) and the National Key Research and Development Programme of the Ministry of Science of Technology of China (grant no. 2022YFC3701101). We would like to express our gratitude to the University of Leeds for providing the Master Chemical Mechanism and to NCAR for the Tropospheric Ultraviolet Visible (TUV) radiation model. We also thank Yaqiang Wang for developing the open-source software MeteoInfo.

Author contributing

LX and HS conceptualized the research. XZ drafted the initial manuscript and analyzed the data. CD supported funding the observation. YZ, CD, and XW designed the field campaign. MZ, JZ, YS, YL, YS, HL, and JM conducted the field campaign. JZ and YL analyzed the aerosol samples and VOC samples, respectively. MZ and YZ assisted with the model simulation. YY, YN, and JT contributed to figure creation. LX, HS, MG, and WW revised the original manuscript.

Competing interests

The authors declare that they have no conflict of interest.

Data availability

The data supporting this study are available upon request from the corresponding author.

References

Acker, K., Möller, D., Wieprecht, W., Meixner, F. X., Bohn, B., Gilge, S., Plass-Dülmer, C., and Berresheim, H.: Strong daytime production of OH from HNO$_2$ at a rural mountain site, Geophys. Res. Lett., 33, 4, 10.1029/2005gl024643, 2006.

Alicke, B., Geyer, A., Hofzumahaus, A., Holland, F., Konrad, S., Pätz, H. W., Schäfer, J., Stutz, J., Volz-Thomas, A., and Platt, U.: OH formation by HONO photolysis during the BERLIOZ experiment, J. Geophys. Res. Atmos., 108, 8247, 10.1029/2001JD000579, 2003.

Altieri, K. E., Fawcett, S. E., Peters, A. J., Sigman, D. M., and Hastings, M. G.: Marine biogenic source of atmospheric organic nitrogen in the subtropical North Atlantic, P. Natl. Acad. Sci., 113, 925-930, 10.1073/pnas.1516847113, 2016.

Andersen, S. T., Carpenter, L. J., Reed, C., Lee, J. D., Chance, R., Sherwen, T., Vaughan, A. R., Stewart, J., Edwards, P. M., Bloss, W. J., Sommariva, R., Crilley, L. R., Nott, G. J., Neves, L., Read, K., Heard, D. E., Seakins, P. W., Whalley, L. K., Boustead, G. A., Fleming, L. T., Stone, D., and Fomba, K. W.: Extensive field evidence for the release of HONO from the photolysis of nitrate aerosols, Science Advances, 9, 10.1126/sciadv.add6266, 2023.

Aumont, B., Chervier, F., and Laval, S.: Contribution of HONO sources to the NO$_x$/HO$_x$/O$_3$ chemistry in the polluted boundary layer, Atmos. Environ., 37, 487-498, 2003.

Broske, R., Kleffmann, J., and Wiesen, P.: Heterogeneous conversion of NO$_2$ on secondary organic aerosol surfaces: A possible source of nitrous acid (HONO) in the atmosphere?, Atmos. Chem. Phys., 3, 469-474, 2003.

Bruggemann, M., Hayeck, N., and George, C.: Interfacial photochemistry at the ocean surface is a global source of organic vapors and aerosols, Nat Commun, 9, 2101, 10.1038/s41467-018-04528-7, 2018.

Crilley, L. R., Kramer, L. J., Pope, F. D., Reed, C., Lee, J. D., Carpenter, L. J., Hollis, L. D. J., Ball, S. M., and Bloss, W. J.: Is the ocean surface a source of nitrous acid (HONO) in the marine boundary layer?, Atmos. Chem. Phys., 21, 18213-18225, 10.5194/acp-21-18213-2021, 2021.

Cui, L. L., Li, R., Fu, H. B., Li, Q., Zhang, L. W., George, C., and Chen, J. M.: Formation features of nitrous acid in the offshore area of the East China Sea, Sci. Total Environ., 682, 138-150, 10.1016/j.scitotenv.2019.05.004, 2019.

Czader, B. H., Rappenglück, B., Percell, P., Byun, D. W., Ngan, F., and Kim, S.: Modeling nitrous acid and its impact on ozone and hydroxyl radical during the Texas Air Quality Study 2006, Atmos. Chem. Phys., 12, 6939-6951, 10.5194/acp-12-6939-2012, 2012.

Donaldson, D. J. and George, C.: Sea-Surface Chemistry and Its Impact on the Marine Boundary Layer, Environ. Sci. Technol., 46, 10385-10389, 10.1021/es301651m, 2012.

Elshorbany, Y. F., Steil, B., Brühl, C., and Lelieveld, J.: Impact of HONO on global atmospheric chemistry calculated with an empirical parameterization in the EMAC model, Atmos. Chem. Phys., 12, 9977-10000, 10.5194/acp-12-9977-2012, 2012.

Ge, S., Wang, G., Zhang, S., Li, D., Xie, Y., Wu, C., Yuan, Q., Chen, J., and Zhang, H.: Abundant NH$_3$ in China Enhances Atmospheric HONO Production by Promoting the Heterogeneous Reaction of SO$_2$ with NO$_2$, Environ. Sci. Technol., 53, 14339-14347, 10.1021/acs.est.9b04196, 2019.

Gen, M., Liang, Z., Zhang, R., Go Mabato, B. R., and Chan, C. K.: Particulate nitrate photolysis in the atmosphere, Environ. Sci. Atmos., 10.1039/D1EA00087J, 2022.

Gu, R., Shen, H., Xue, L., Wang, T., Gao, J., Li, H., Liang, Y., Xia, M., Yu, C., Liu, Y., and Wang, W.: Investigating the sources of atmospheric nitrous acid (HONO) in the megacity of Beijing, China, Sci. Total Environ., 812, 152270, 10.1016/j.scitotenv.2021.152270, 2022a.

Gu, R., Wang, W., Peng, X., Xia, M., Zhao, M., Zhang, Y., Wang, Y. n., Liu, Y., Shen, H., Xue, L., Wang, T., and Wang, W.: Nitrous acid in the polluted coastal atmosphere of the South China Sea: Ship emissions, budgets, and impacts, Sci. Total Environ., 826, 153692, 10.1016/j.scitotenv.2022.153692, 2022b.

Hao, Q., Jiang, N., Zhang, R., Yang, L., and Li, S.: Characteristics, sources, and reactions of nitrous acid during winter at an urban site in the Central Plains Economic Region in China, Atmos. Chem. Phys., 20, 7087-7102, 10.5194/acp-20-7087-2020, 2020.

Harrison, R. M. and Kitto, A.-M. N.: Evidence for a surface source of atmospheric nitrous acid, Atmos. Environ., 28, 1089-1094, 10.1016/1352-2310(94)90286-0, 1994.

Jenkin, M. E., Young, J. C., and Rickard, A. R.: The MCM v3.3.1 degradation scheme for isoprene, Atmos. Chem. Phys., 15, 11433-11459, 10.5194/acp-15-11433-2015, 2015.

Jiang, Y., Xue, L., Shen, H., Dong, C., Xiao, Z., and Wang, W.: Dominant Processes of HONO Derived from Multiple Field Observations in Contrasting Environments, Environ. Sci. Technol. Lett., 9, 258-264, 10.1021/acs.estlett.2c00004, 2022.

Jiang, Y., Hoffmann, E. H., Tilgner, A., Aiyuk, M. B. E., Andersen, S. T., Wen, L., van Pinxteren, M., Shen, H., Xue, L., Wang, W., and Herrmann, H.: Insights into NOx and HONO chemistry in the tropical marine boundary layer at Cape Verde during the MarParCloud campaign, J. Geophys. Res. Atmos., 10.1029/2023jd038865, 2023.

Jiang, Y., Xue, L., Gu, R., Jia, M., Zhang, Y., Wen, L., Zheng, P., Chen, T., Li, H., Shan, Y., Zhao, Y., Guo, Z., Bi, Y., Liu, H., Ding, A., Zhang, Q., and Wang, W.: Sources of nitrous acid (HONO) in the upper boundary layer and lower free troposphere of the North China Plain: insights from the Mount Tai Observatory, Atmos. Chem. Phys., 20, 12115-12131, 10.5194/acp-20-12115-2020, 2020.

Kasibhatla, P., Sherwen, T., Evans, M. J., Carpenter, L. J., Reed, C., Alexander, B., Chen, Q. J., Sulprizio, M. P., Lee, J. D., Read, K. A., Bloss, W., Crilley, L. R., Keene, W. C., Pszenny, A. A. P., and Hodzic, A.: Global impact of nitrate photolysis in sea-salt aerosol on NO_x, OH, and O_3 in the marine boundary layer, Atmos. Chem. Phys., 18, 11185-11203, 10.5194/acp-18-11185-2018, 2018.

Kebede, M. A., Bish, D. L., Losovyj, Y., Engelhard, M. H., and Raff, J. D.: The Role of Iron-Bearing Minerals in NO_2 to HONO Conversion on Soil Surfaces, Environ. Sci. Technol., 50, 8649-8660, 10.1021/acs.est.6b01915, 2016.

Kleffmann, J.: Daytime sources of nitrous acid (HONO) in the atmospheric boundary layer, Chemphyschem, 8, 1137-1144, 10.1002/cphc.200700016, 2007.

Kleffmann, J., Becker, K., and Wiesen, P.: Heterogeneous NO_2 conversion processes on acid surfaces: possible atmospheric implications, Atmos. Environ., 32, 2721-2729, 1998.

Kleffmann, J., Kurtenbach, R., Lörzer, J., Wiesen, P., Kalthoff, N., Vogel, B., and Vogel, H.: Measured and simulated vertical profiles of nitrous acid—Part I: Field measurements, Atmos. Environ., 37, 2949-2955, 10.1016/s1352-2310(03)00242-5, 2003.

Kleffmann, J., Gavriloaiei, T., Hofzumahaus, A., Holland, F., Koppmann, R., Rupp, L., Schlosser, E., Siese, M., and Wahner, A.: Daytime formation of nitrous acid: A major source of OH radicals in a forest, Geophys. Res. Lett., 32, L05818, 10.1029/2005gl022524, 2005.

Kramer, L. J., Crilley, L. R., Adams, T. J., Ball, S. M., Pope, F. D., and Bloss, W. J.: Nitrous acid (HONO) emissions under real-world driving conditions from vehicles in a UK road tunnel, Atmos. Chem. Phys., 20, 5231-5248, 10.5194/acp-20-5231-2020, 2020.

Kurtenbach, R., Becker, K. H., Gomes, J. A. G., Kleffmann, J., Lorzer, J. C., Spittler, M., Wiesen, P., Ackermann, R., Geyer, A., and Platt, U.: Investigations of emissions and heterogeneous formation of HONO in a road traffic tunnel, Atmos. Environ., 35, 3385-3394, 10.1016/s1352-2310(01)00138-8, 2001.

Lee, J. D., Whalley, L. K., Heard, D. E., Stone, D., Dunmore, R. E., Hamilton, J. F., Young, D. E., Allan, J. D., Laufs, S., and Kleffmann, J.: Detailed budget analysis of HONO in central London reveals a missing daytime source, Atmos. Chem. Phys., 16, 2747-2764, 10.5194/acp-16-2747-2016, 2016.

Lelièvre, S., Bedjanian, Y., Laverdet, G., and Le Bras, G.: Heterogeneous reaction of NO_2 with hydrocarbon flame soot, J. Phys. Chem. A, 108, 10807-10817, 2004.

Li, D., Xue, L., Wen, L., Wang, X., Chen, T., Mellouki, A., Chen, J., and Wang, W.: Characteristics and sources of nitrous acid in an urban atmosphere of northern China: Results from 1-yr continuous observations, Atmos. Environ., 182, 296-306, 10.1016/j.atmosenv.2018.03.033, 2018a.

Li, L., Duan, Z., Li, H., Zhu, C., Henkelman, G., Francisco, J. S., and Zeng, X. C.: Formation of HONO from the NH_3-promoted hydrolysis of NO_2 dimers in the atmosphere, P. Natl. Acad. Sci., 115, 7236-7241, 10.1073/pnas.1807719115, 2018b.

Li, M., Su, H., Li, G., Ma, N., Pöschl, U., and Cheng, Y.: Relative importance of gas uptake on aerosol and ground surfaces characterized by equivalent uptake coefficients, Atmos. Chem. Phys., 19, 10981-11011, 10.5194/acp-19-10981-2019, 2019.

Liao, S., Zhang, J., Yu, F., Zhu, M., Liu, J., Ou, J., Dong, H., Sha, Q., Zhong, Z., Xie, Y., Luo, H., Zhang, L., and Zheng, J.: High Gaseous Nitrous Acid (HONO) Emissions from Light-Duty Diesel Vehicles, Environ. Sci. Technol., 55, 200-208, 10.1021/acs.est.0c05599, 2021.

Liu, C.-M., Young, C.-Y., and Lee, Y.-C.: Influence of Asian dust storms on air quality in Taiwan, Sci. Total Environ., 368, 884-897, 10.1016/j.scitotenv.2006.03.039, 2006.

Liu, J., Li, S., Mekic, M., Jiang, H., Zhou, W., Loisel, G., Song, W., Wang, X., and Gligorovski, S.: Photoenhanced Uptake of NO_2 and HONO Formation on Real Urban Grime, Environ. Sci. Technol. Lett., 6, 413-417, 10.1021/acs.estlett.9b00308, 2019a.

Liu, T. and Abbatt, J. P. D.: Oxidation of sulfur dioxide by nitrogen dioxide accelerated at the interface of deliquesced aerosol particles, Nat Chem, 13, 1173-1177, 10.1038/s41557-021-00777-0, 2021.

Liu, Y., Shen, H., Mu, J., Li, H., Chen, T., Yang, J., Jiang, Y., Zhu, Y., Meng, H., Dong, C., Wang, W., and Xue, L.: Formation of peroxyacetyl nitrate (PAN) and its impact on ozone production in the coastal atmosphere of Qingdao, North China, Sci. Total Environ., 778, 146265, 10.1016/j.scitotenv.2021.146265, 2021.

Liu, Y. H., Lu, K. D., Li, X., Dong, H. B., Tan, Z. F., Wang, H. C., Zou, Q., Wu, Y. S., Zeng, L. M., Hu, M., Min, K. E., Kecorius, S., Wiedensohler, A., and Zhang, Y. H.: A Comprehensive Model Test of the HONO Sources Constrained to Field Measurements at Rural North China Plain, Environ. Sci. Technol., 53, 3517-3525, 10.1021/acs.est.8b06367, 2019b.

Ma, Q., Wang, T., Liu, C., He, H., Wang, Z., Wang, W., and Liang, Y.: SO_2 Initiates the Efficient Conversion of NO_2 to HONO on MgO Surface, Environ Sci Technol, 51, 3767-3775, 10.1021/acs.est.6b05724, 2017.

Meusel, H., Kuhn, U., Reiffs, A., Mallik, C., Harder, H., Martinez, M., Schuladen, J., Bohn, B., Parchatka, U., Crowley, J. N., Fischer, H., Tomsche, L., Novelli, A., Hoffmann, T., Janssen, R. H. H., Hartogensis, O., Pikridas, M., Vrekoussis, M., Bourtsoukidis, E., Weber, B., Lelieveld, J., Williams, J., Poschl, U., Cheng, Y. F., and Su, H.: Daytime formation of nitrous acid at a coastal remote site in Cyprus indicating a common ground source of atmospheric HONO and NO, Atmos. Chem. Phys., 16, 14475-14493, 10.5194/acp-16-14475-2016, 2016.

Nie, W., Ding, A. J., Xie, Y. N., Xu, Z., Mao, H., Kerminen, V. M., Zheng, L. F., Qi, X. M., Huang, X., Yang, X. Q., Sun, J. N., Herrmann, E., Petäjä, T., Kulmala, M., and Fu, C. B.: Influence of biomass burning plumes on HONO chemistry in eastern China, Atmos. Chem. Phys., 15, 1147-1159, 10.5194/acp-15-1147-2015, 2015.

Reed, C., Evans, M. J., Crilley, L. R., Bloss, W. J., Sherwen, T., Read, K. A., Lee, J. D., and Carpenter, L. J.: Evidence for renoxification in the tropical marine boundary layer, Atmos. Chem. Phys., 17, 4081-4092, 10.5194/acp-17-4081-2017, 2017.

Romer, P. S., Wooldridge, P. J., Crounse, J. D., Kim, M. J., Wennberg, P. O., Dibb, J. E., Scheuer, E., Blake, D. R., Meinardi, S., Brosius, A. L., Thames, A. B., Miller, D. O., Brune, W. H., Hall, S. R., Ryerson, T. B., and Cohen, R. C.: Constraints on Aerosol Nitrate Photolysis as a Potential Source of HONO and NO_x, Environ. Sci. Technol., 52, 13738-13746, 10.1021/acs.est.8b03861, 2018.

Shi, Q., Tao, Y., Krechmer, J. E., Heald, C. L., Murphy, J. G., Kroll, J. H., and Ye, Q.: Laboratory Investigation of Renoxification from the Photolysis of Inorganic Particulate Nitrate, Environ. Sci. Technol., 55, 854-861, 10.1021/acs.est.0c06049, 2021.

Stemmler, K., Ammann, M., Donders, C., Kleffmann, J., and George, C.: Photosensitized reduction of nitrogen dioxide on humic acid as a source of nitrous acid, Nature, 440, 195-198, 10.1038/nature04603, 2006.

Stemmler, K., Ndour, M., Elshorbany, Y., Kleffmann, J., D'Anna, B., George, C., Bohn, B., and Ammann, M.: Light induced conversion of nitrogen dioxide into nitrous acid on submicron humic acid aerosol, Atmos. Chem. Phys., 7, 4237-4248, 10.5194/acp-7-4237-2007, 2007.

Su, H., Cheng, Y. F., Shao, M., Gao, D. F., Yu, Z. Y., Zeng, L. M., Slanina, J., Zhang, Y. H., and Wiedensohler, A.: Nitrous acid (HONO) and its daytime sources at a rural site during the 2004 PRIDE-PRD experiment in China, J. Geophys. Res. Atmos., 113, 10.1029/2007JD009060, 2008.

Su, H., Cheng, Y., Oswald, R., Behrendt, T., Trebs, I., Meixner, F. X., Andreae, M. O., Cheng, P., Zhang, Y., and Poschl, U.: Soil nitrite as a source of atmospheric HONO and OH radicals, Science, 333, 1616-1618, 10.1126/science.1207687, 2011.

Tang, Y., An, J., Wang, F., Li, Y., Qu, Y., Chen, Y., and Lin, J.: Impacts of an unknown daytime HONO source on the mixing ratio and budget of HONO, and hydroxyl, hydroperoxyl, and organic peroxy radicals, in the coastal regions of China, Atmos. Chem. Phys., 15, 9381-9398, 10.5194/acp-15-9381-2015, 2015.

Theys, N., Volkamer, R., Müller, J. F., Zarzana, K. J., Kille, N., Clarisse, L., De Smedt, I., Lerot, C., Finkenzeller, H., Hendrick, F., Koenig, T. K., Lee, C. F., Knote, C., Yu, H., and Van Roozendael, M.: Global nitrous acid emissions and levels of regional oxidants enhanced by wildfires, Nat. Geosci., 13, 681-686, 10.1038/s41561-020-0637-7, 2020.

Tong, S., Hou, S., Zhang, Y., Chu, B., Liu, Y., He, H., Zhao, P., and Ge, M.: Exploring the nitrous acid (HONO) formation mechanism in winter Beijing: direct emissions and heterogeneous production in urban and suburban areas, Faraday Discuss., 189, 213-230, 10.1039/c5fd00163c, 2016.

Underwood, G. M., Song, C. H., Phadnis, M., Carmichael, G. R., and Grassian, V. H.: Heterogeneous reactions of NO_2 and HNO_3 on oxides and mineral dust: A combined laboratory and modeling study, J. Geophys. Res. Atmos., 106, 18055-18066, 10.1029/2000JD900552, 2001.

VandenBoer, T. C., Brown, S. S., Murphy, J. G., Keene, W. C., Young, C. J., Pszenny, A. A. P., Kim, S., Warneke, C., de Gouw, J. A., Maben, J. R., Wagner, N. L., Riedel, T. P., Thornton, J. A., Wolfe, D. E., Dubé, W. P., Öztürk, F., Brock, C. A., Grossberg, N., Lefer, B., Lerner, B., Middlebrook, A. M., and Roberts, J. M.: Understanding the role of the ground surface in HONO vertical structure: High resolution vertical profiles during NACHTT-11, J. Geophys. Res. Atmos., 118, 10,155-110,171, 10.1002/jgrd.50721, 2013.

Villena, G., Wiesen, P., Cantrell, C. A., Flocke, F., Fried, A., Hall, S. R., Hornbrook, R. S., Knapp, D., Kosciuch, E., Mauldin, R. L., McGrath, J. A., Montzka, D., Richter, D., Ullmann, K., Walega, J., Weibring, P., Weinheimer, A., Staebler, R. M., Liao, J., Huey, L. G., and Kleffmann, J.: Nitrous acid (HONO) during polar spring in Barrow, Alaska: A net source of OH radicals?, J. Geophys. Res., 116, D00R07, 10.1029/2011jd016643, 2011.

Vogel, B., Vogel, H., Kleffmann, J., and Kurtenbach, R.: Measured and simulated vertical profiles of nitrous acid—Part II. Model simulations and indications for a photolytic source, Atmos. Environ., 37, 2957-2966, 10.1016/s1352-2310(03)00243-7, 2003.

Wang, S.: Atmospheric observations of enhanced NO_2-HONO conversion on mineral dust particles, Geophys. Res. Lett., 30, 10.1029/2003gl017014, 2003.

Wang, Y. Q.: MeteoInfo: GIS software for meteorological data visualization and analysis, MeApp, 21, 360-368, 10.1002/met.1345, 2012.

Wojtal, P., Halla, J. D., and McLaren, R.: Pseudo steady states of HONO measured in the nocturnal marine boundary layer: a conceptual model for HONO formation on aqueous surfaces, Atmos. Chem. Phys., 11, 3243-3261, 10.5194/acp-11-3243-2011, 2011.

Wu, C., Zhang, S., Wang, G., Lv, S., Li, D., Liu, L., Li, J., Liu, S., Du, W., Meng, J., Qiao, L., Zhou, M., Huang, C., and Wang, H.: Efficient Heterogeneous Formation of Ammonium Nitrate on the Saline Mineral Particle Surface in the Atmosphere of East Asia during Dust Storm Periods, Environ. Sci. Technol., 54, 15622-15630, 10.1021/acs.est.0c04544, 2020.

Wurl, O., Stolle, C., Van Thuoc, C., The Thu, P., and Mari, X.: Biofilm-like properties of the sea surface and predicted effects on air–sea CO_2 exchange, Prog. Oceanogr., 144, 15-24, 10.1016/j.pocean.2016.03.002, 2016.

Xing, L., Wu, J., Elser, M., Tong, S., Liu, S., Li, X., Liu, L., Cao, J., Zhou, J., El-Haddad, I., Huang, R., Ge, M., Tie, X., Prévôt, A. S. H., and Li, G.: Wintertime secondary organic aerosol formation in Beijing–Tianjin–Hebei (BTH): contributions of HONO sources and heterogeneous reactions, Atmos. Chem. Phys., 19, 2343-2359, 10.5194/acp-19-2343-2019, 2019.

Xue, C., Ye, C., Kleffmann, J., Zhang, C., Catoire, V., Bao, F., Mellouki, A., Xue, L., Chen, J., Lu, K., Zhao, Y., Liu, H., Guo, Z., and Mu, Y.: Atmospheric measurements at Mt. Tai—Part I: HONO formation and its role in the oxidizing capacity of the upper boundary layer, Atmos. Chem. Phys., 22, 3149-3167, 10.5194/acp-22-3149-2022, 2022.

Xue, C., Zhang, C., Ye, C., Liu, P., Catoire, V., Krysztofiak, G., Chen, H., Ren, Y., Zhao, X., Wang, J., Zhang, F., Zhang, C., Zhang, J., An, J., Wang, T., Chen, J., Kleffmann, J., Mellouki, A., and Mu, Y.: HONO Budget and Its Role in Nitrate Formation in the Rural North China Plain, Environ. Sci. Technol., 54, 11048-11057, 10.1021/acs.est.0c01832, 2020a.

Xue, C. Y., Zhang, C. L., Ye, C., Liu, P. F., Catoire, V., Krysztofiak, G., Chen, H., Ren, Y. G., Zhao, X. X., Wang, J. H., Zhang, F., Zhang, C. X., Zhang, J. W., An, J. L., Wang, T., Chen, J. M., Kleffmann, J., Mellouki, A., and Mu, Y. J.: HONO Budget and Its Role in Nitrate Formation in the Rural North China Plain, Environ. Sci. Technol., 54, 11048-11057, 10.1021/acs.est.0c01832, 2020b.

Xue, L. K., Wang, T., Gao, J., Ding, A. J., Zhou, X. H., Blake, D. R., Wang, X. F., Saunders, S. M., Fan, S. J., Zuo, H. C., Zhang, Q. Z., and Wang, W. X.: Ground-level ozone in four Chinese cities: precursors, regional transport and heterogeneous processes, Atmos. Chem. Phys., 14, 13175-13188, 10.5194/acp-14-13175-2014, 2014.

Yabushita, A., Enami, S., Sakamoto, Y., Kawasaki, M., Hoffmann, M., and Colussi, A.: Anion-catalyzed dissolution of NO_2 on aqueous microdroplets, J. Phys. Chem. A, 113, 4844-4848, 2009.

Yang, J., Shen, H., Guo, M.-Z., Zhao, M., Jiang, Y., Chen, T., Liu, Y., Li, H., Zhu, Y., Meng, H., Wang, W., and Xue, L.: Strong marine-derived nitrous acid (HONO) production observed in the coastal atmosphere of northern China, Atmos. Environ., 244, 10.1016/j.atmosenv.2020.117948, 2021a.

Yang, X., Xue, L., Wang, T., Wang, X., Gao, J., Lee, S., Blake, D. R., Chai, F., and Wang, W.: Observations and Explicit Modeling of Summertime Carbonyl Formation in Beijing: Identification of Key Precursor Species and Their Impact on Atmospheric Oxidation Chemistry, J. Geophys. Res. Atmos., 123, 1426-1440, 10.1002/2017jd027403, 2018.

Yang, Y., Li, X., Zu, K., Lian, C., Chen, S., Dong, H., Feng, M., Liu, H., Liu, J., Lu, K., Lu, S., Ma, X., Song, D., Wang, W., Yang, S., Yang, X., Yu, X., Zhu, Y., Zeng, L., Tan, Q., and Zhang, Y.: Elucidating the effect of HONO on O_3 pollution by a case study in southwest China, Sci. Total Environ., 756, 144127, 10.1016/j.scitotenv.2020.144127, 2021b.

Ye, C., Zhang, N., Gao, H., and Zhou, X.: Photolysis of Particulate Nitrate as a Source of HONO and NO_x, Environ. Sci. Technol., 51, 6849-6856, 10.1021/acs.est.7b00387, 2017.

Ye, C., Zhou, X., Pu, D., Stutz, J., Festa, J., Spolaor, M., Tsai, C., Cantrell, C., Mauldin, R. L., 3rd, Campos, T., Weinheimer, A., Hornbrook, R. S., Apel, E. C., Guenther, A., Kaser, L., Yuan, B., Karl, T., Haggerty, J., Hall, S., Ullmann, K., Smith, J. N., Ortega, J., and Knote, C.: Rapid cycling of reactive nitrogen in the marine boundary layer, Nature, 532, 489-491, 10.1038/nature17195, 2016a.

Ye, C. X., Gao, H. L., Zhang, N., and Zhou, X. L.: Photolysis of Nitric Acid and Nitrate on Natural and Artificial Surfaces, Environ. Sci. Technol., 50, 3530-3536, 10.1021/acs.est.5b05032, 2016b.

Yu, C., Wang, Z., Ma, Q., Xue, L., George, C., and Wang, T.: Measurement of heterogeneous uptake of NO_2 on inorganic particles, sea water and urban grime, J. Environ. Sci., 106, 124-135, 10.1016/j.jes.2021.01.018, 2021.

Yu, C., Huang, L., Xue, L., Shen, H., Li, Z., Zhao, M., Yang, J., Zhang, Y., Li, H., Mu, J., and Wang, W.: Photoenhanced Heterogeneous Uptake of NO_2 and HONO Formation on Authentic Winter Time Urban Grime, ACS Earth Space Chem., 6, 1960-1968, 10.1021/acsearthspacechem.2c00054, 2022a.

Yu, Y., Cheng, P., Li, H., Yang, W., Han, B., Song, W., Hu, W., Wang, X., Yuan, B., Shao, M., Huang, Z., Li, Z., Zheng, J., Wang, H., and Yu, X.: Budget of nitrous acid (HONO) at an urban site in the fall season of Guangzhou, China, Atmos. Chem. Phys., 22, 8951-8971, 10.5194/acp-22-8951-2022, 2022b.

Zha, Q. Z., Xue, L. K., Wang, T., Xu, Z., Yeung, C. P., Louie, P. K. K., and Luk, C. W. Y.: Large conversion rates of NO_2 to HNO_2 observed in air masses from the South China Sea: Evidence of strong production at sea surface?, Geophys. Res. Lett., 41, 7710-7715, 10.1002/2014gl061429, 2014.

Zhang, Q., Liu, P., Wang, Y., George, C., Chen, T., Ma, S., Ren, Y., Mu, Y., Song, M., Herrmann, H., Mellouki, A., Chen, J., Yue, Y., Zhao, X., Wang, S., and Zeng, Y.: Unveiling the underestimated direct emissions of nitrous acid (HONO), P. Natl. Acad. Sci., 120, e2302048120, 10.1073/pnas.2302048120, 2023.

Zhang, R., Gen, M., Huang, D., Li, Y., and Chan, C. K.: Enhanced Sulfate Production by Nitrate Photolysis in the Presence of Halide Ions in Atmospheric Particles, Environ. Sci. Technol., 54, 3831-3839, 10.1021/acs.est.9b06445, 2020.

Zhang, W., Tong, S., Ge, M., An, J., Shi, Z., Hou, S., Xia, K., Qu, Y., Zhang, H., Chu, B., Sun, Y., and He, H.: Variations and sources of nitrous acid (HONO) during a severe pollution episode in Beijing in winter 2016, Sci. Total Environ., 648, 253-262, 10.1016/j.scitotenv.2018.08.133, 2019.

Zhang, X., Tong, S., Jia, C., Zhang, W., Li, J., Wang, W., Sun, Y., Wang, X., Wang, L., Ji, D., Wang, L., Zhao, P., Tang, G., Xin, J., Li, A., and Ge, M.: The Levels and Sources of Nitrous Acid (HONO) in Winter of Beijing and Sanmenxia, J. Geophys. Res. Atmos., 127, 10.1029/2021jd036278, 2022.

Zhou, X., Zhang, N., TerAvest, M., Tang, D., Hou, J., Bertman, S., Alaghmand, M., Shepson, P. B., Carroll, M. A., Griffith, S., Dusanter, S., and Stevens, P. S.: Nitric acid photolysis on forest canopy surface as a source for tropospheric nitrous acid, Nat. Geosci., 4, 440-443, 10.1038/ngeo1164, 2011.

Zhou, X. L., Gao, H. L., He, Y., Huang, G., Bertman, S. B., Civerolo, K., and Schwab, J.: Nitric acid photolysis on surfaces in low-NO_x environments: Significant atmospheric implications, Geophys. Res. Lett., 30, 10.1029/2003gl018620, 2003.

Zhu, Y., Wang, Y., Zhou, X., Elshorbany, Y. F., Ye, C., Hayden, M., and Peters, A. J.: An investigation into the chemistry of HONO in the marine boundary layer at Tudor Hill Marine Atmospheric Observatory in Bermuda, Atmos. Chem. Phys., 22, 6327-6346, 10.5194/acp-22-6327-2022, 2022.

Figures and Tables
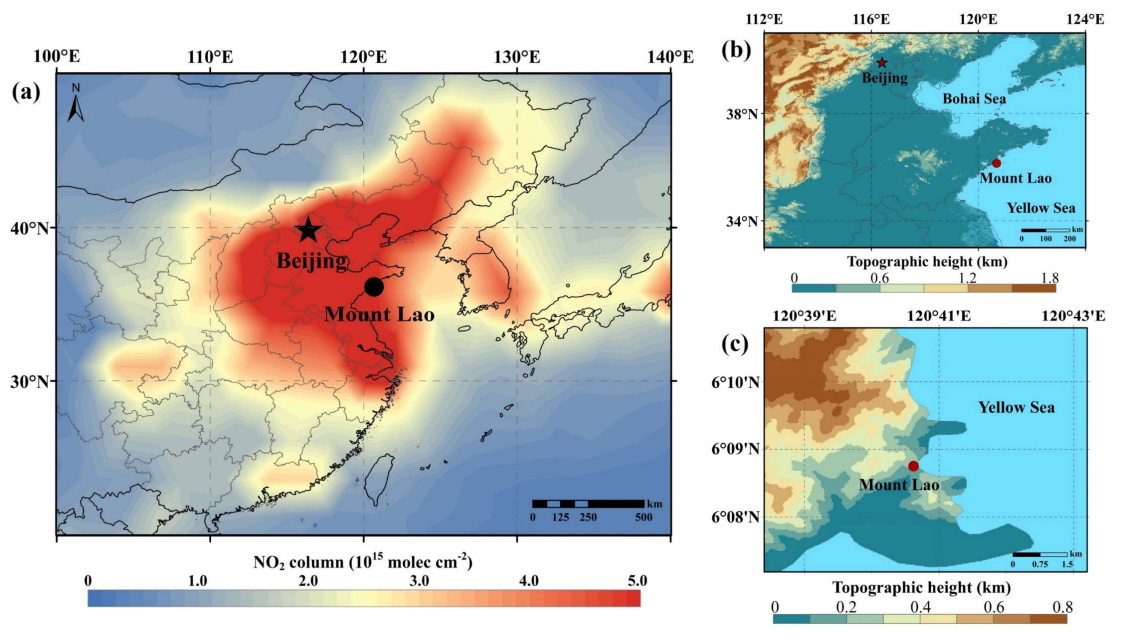
Figure 1. Maps showing the location of the monitoring site. Figure 1a is colored by tropospheric NO_2 column density in May 2021 from the Ozone Monitoring Instrument (OMI, https://www.earthdata.nasa.gov/), and Figure 1b and Figure 1c are colored by the geographical height from the Geospatial Data Cloud (http://www.gscloud.cn/).
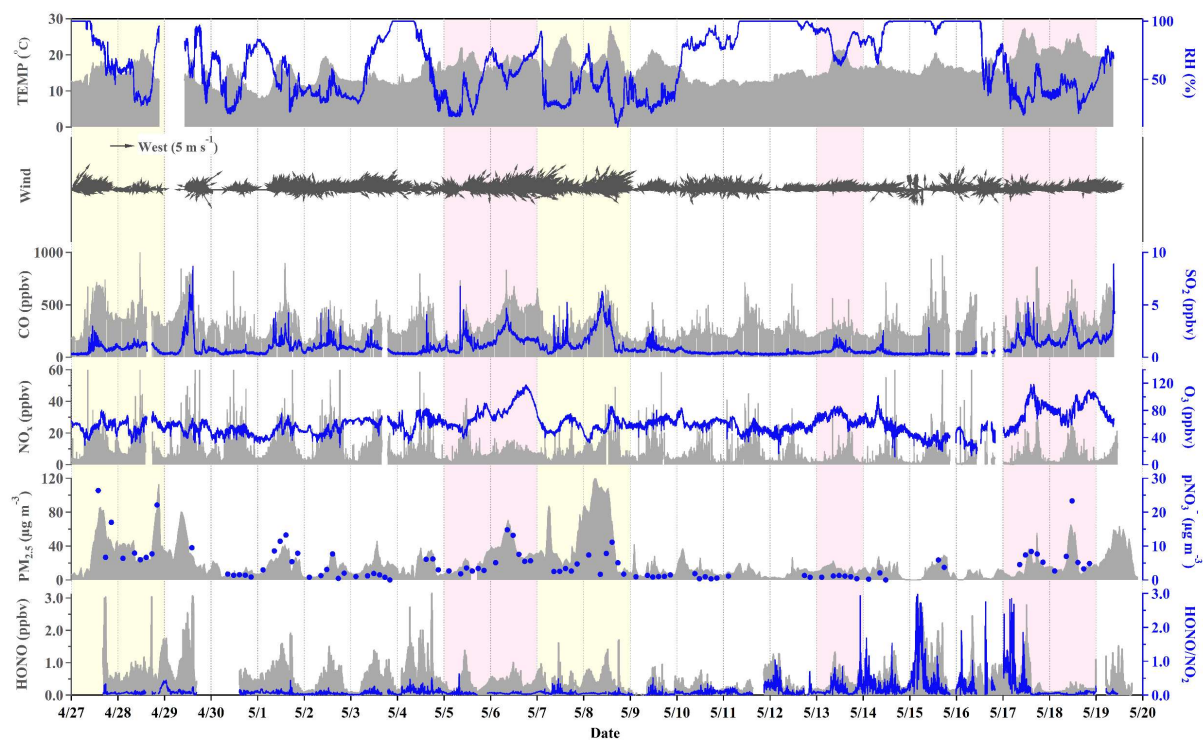
Figure 2. Time series of HONO, meteorological parameters, and related species measured during the campaign. The yellow shaded areas correspond to the period of dust, while the pink shaded areas represent the period of photochemical pollution.

810
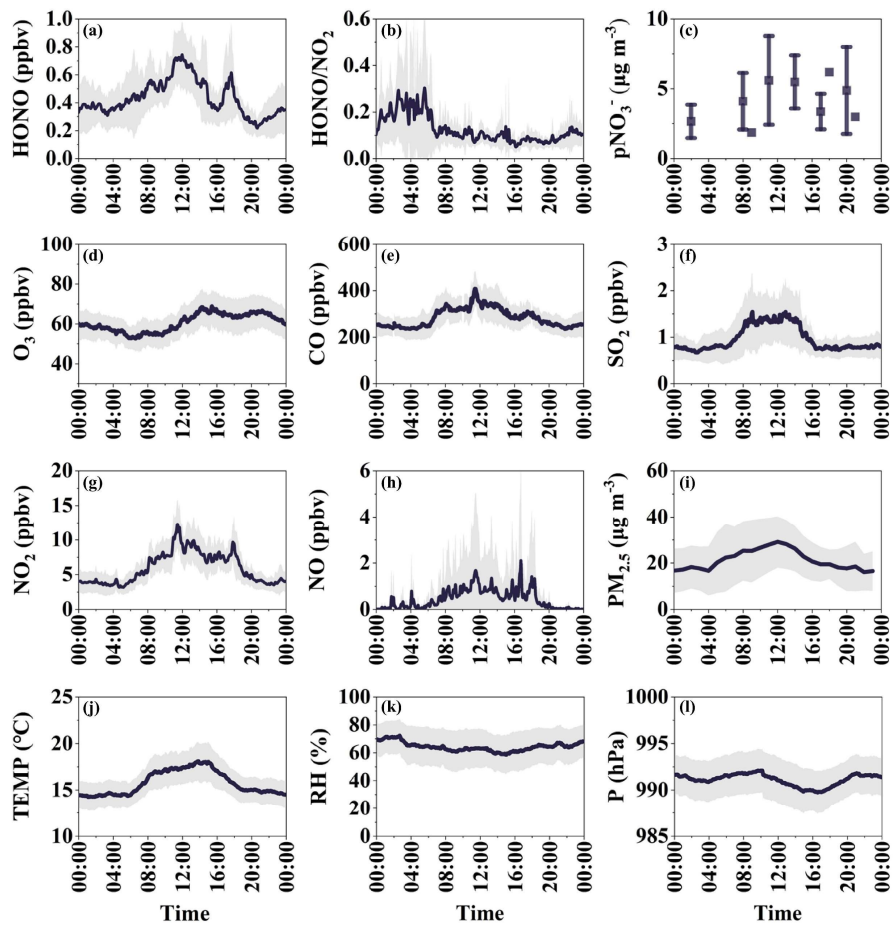
Figure 3. Average diurnal variations of (a) HONO, (b) HONO/NO₂, (c) particle nitrate, (d) O₃, (e) CO, (f) SO₂, (g) NO₂, (h) NO, (i) PM₂.₅, (j) temperature, (k) RH, and (l) pressure during the observation period. The shaded area indicates the range of half of the standard deviation.

814
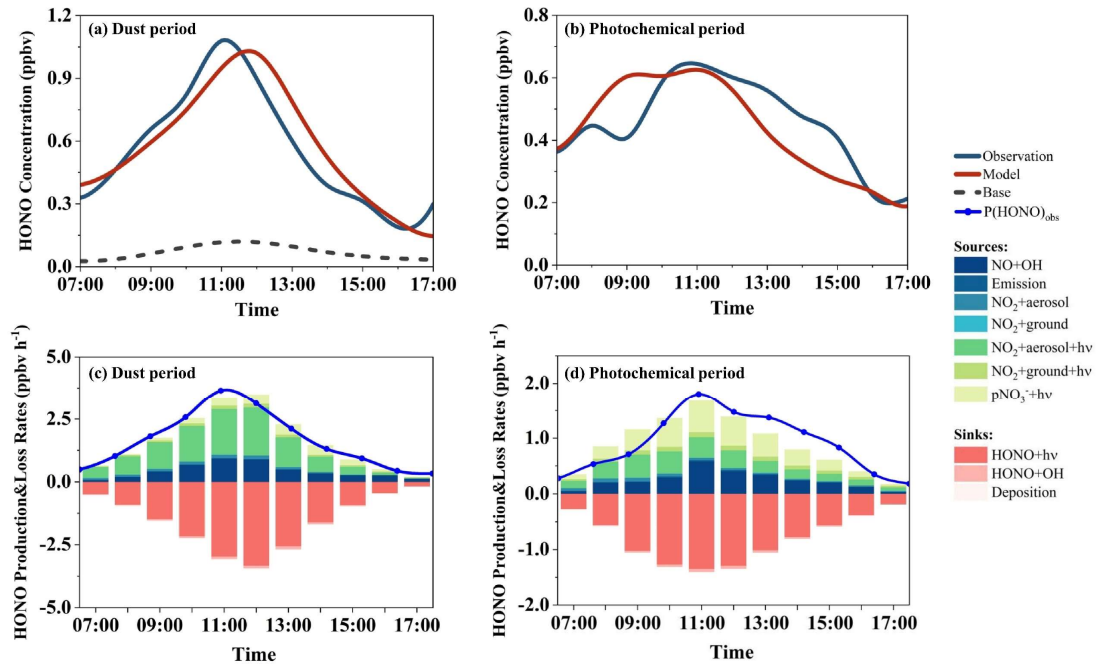
815

816   **Figure 4.** Daytime HONO budgets in dust (a, c) and (b, d) photochemical period at Mount Lao. The

817   base case only considered the homogeneous reaction of NO + OH, and the model case considered the

818   updated HONO sources described in this study.

819
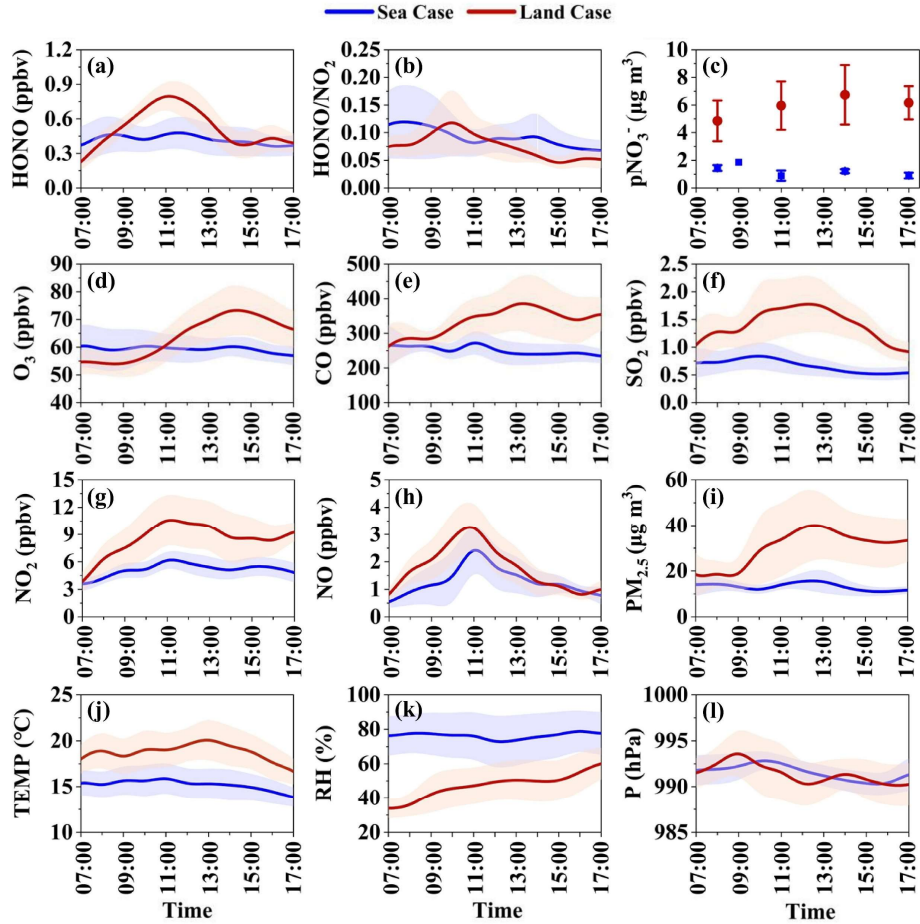
820

821 **Figure 5.** Average diurnal variations of HONO and related parameters in the "sea case" and the "land

822 case" during the campaign at Mount Lao. The shaded area indicates half of the standard deviation.

823
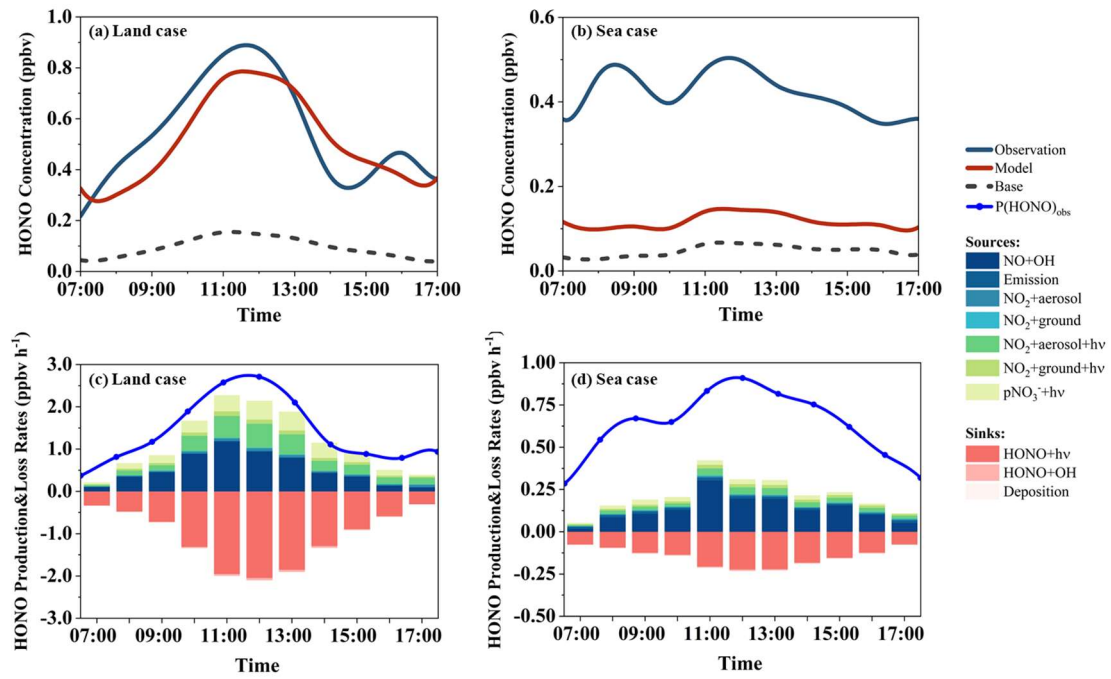
824

825 **Figure 6.** Comparison of the observed and modeled daytime (7:00–17:00) HONO concentrations and

826 modeled HONO budgets in the "land case" (a, c) and the "sea case" (b, d).

827

828
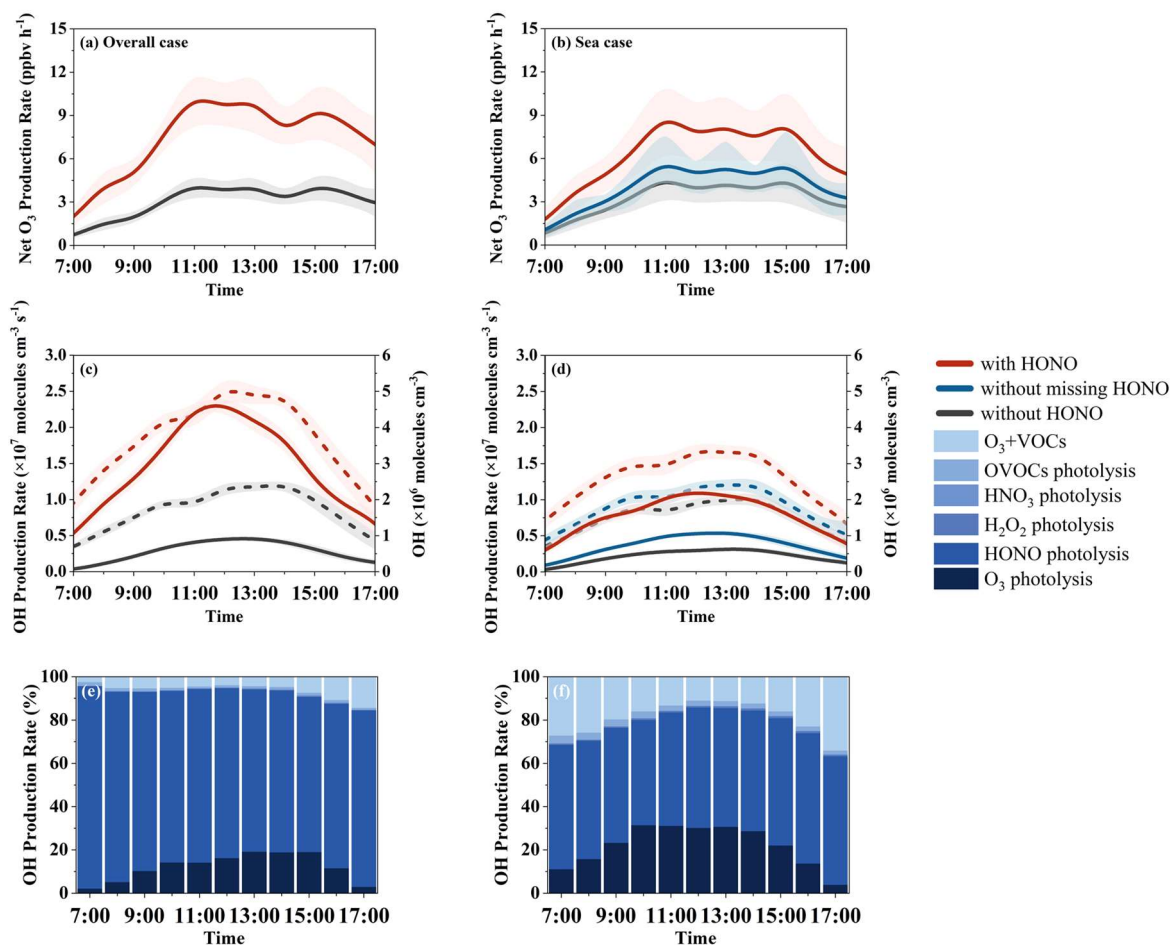
Figure 7. Comparison of simulated net O_3 and OH radical production rate (solid lines) and concentration (dashed lines) with and without HONO measurement data constraints and relative diurnal contributions of different OH radical sources with HONO constrained in the "land case" (a, c, e) and the "sea case" (b, d, f). The shaded area indicates the standard deviation.

833

834 **Table 1**. Summary of HONO source and sinks included in the box model.

Pathways	Parametrization	References
Direct emission	$k_{emission} = 0.8\%$	Kleffmann et al. (2003)
$OH + NO \rightarrow HONO$	k_{OH+NO}	Calculated in model
$NO_2 + H_2O \xrightarrow{\text{aerosol surface}} HONO + HNO_3$	$k = 0.25 \times v_{NO_2} \times Sa \times \gamma_a$ $\gamma_a = 8 \times 10^{-6}$	Vandenboer et al. (2013)
$NO_2 + H_2O \xrightarrow{\text{ground surface}} HONO + HNO_3$	$k = 0.25 \times v_{NO_2} \times \gamma_g \times \frac{S}{V}$ $\gamma_g = 1 \times 10^{-6}, \frac{S}{V} = \frac{1.7}{BLH}$	Kleffmann et al. (1998); Vogel et al. (2003)
$NO_2 + h\nu \xrightarrow{\text{aerosol surface}} HONO$	$k = 0.25 \times v_{NO_2} \times Sa \times \gamma_{a,\,h\nu} \times \frac{JNO_2}{JNO_{2,noon}}$ $\gamma_{a,\,hv} = 4 \times 10^{-5}$	Lelièvre et al. (2004)
$NO_2 + h\nu \xrightarrow{\text{ground surface}} HONO$	$k = 0.25 \times v_{NO_2} \times \gamma_{g,\,h\nu} \times \frac{S}{V} \times \frac{JNO_2}{JNO_{2,noon}}$ $\gamma_{g,\,hv} = 2 \times 10^{-5}, \frac{S}{V} = \frac{1.7}{BLH}$	Stemmler et al. (2006); Vogel et al. (2003)
$pNO_3^- + h\nu \rightarrow HONO$	$k = \frac{8.3 \times 10^{-5}}{7 \times 10^{-7}} \times J(HNO_3)_{MCM}$	Ye et al. (2017)
$HONO + h\nu \rightarrow NO + OH$	$k = J(HONO)$	Calculated in model
$HONO + OH \rightarrow H_2O + NO_2$	$k_{OH+HONO}$	Calculated in model
Deposition	$k = \frac{v_{HONO}}{BLH}$	Calculated in model

835

836 **Table 2.** Statistics of measured species and meteorological parameters during the campaign.

Parameters	Mean	SD	Minimum	Median	Maximum
HONO (ppbv)	0.46	0.37	< DL (0.005)	0.38	3.14
HONO/NO_2	0.13	0.24	–	0.07	2.97
NO (ppbv)	0.9	1.7	0.1	0.2	38.3
NO_2 (ppbv)	5.9	4.8	0.4	4.6	65.1
O_3 (ppbv)	60.4	15.8	11.6	58.8	118.1
CO (ppbv)	284.0	118.8	104.2	250.3	1046.7
SO_2 (ppbv)	1.0	0.8	< DL (0.12)	0.7	8.9
$PM_{2.5}$ ($\mu g\ m^{-3}$)	21.2	21.0	< DL (0.5)	14.4	120.7
Sa ($m^2\ m^{-3}$)	6.2×10^{-4}	5.8×10^{-4}	2.8×10^{-4}	4.2×10^{-4}	3.1×10^{-3}
pNO_3^- ($\mu g\ m^{-3}$)	4.6	5.0	0.02^*	2.8	26.4
TEMP (°C)	15.1	3.4	7.5	15.6	27.9
RH (%)	68.7	26.1	9.0	64.8	99.9
P (kPa)	991.1	4.4	979.0	991.0	1003.0
WS ($m\ s^{-1}$)	1.23	0.96	0^*	1.00	9.30
WD (°)	–	–	0	247	354

837 DL: detection limit.

838

839 **Table 3**. Comparison of the statistics for the measured species and meteorological parameters during
840 dust, photochemical pollution, and non-polluted periods in the daytime (7:00–17:00).

Parameters	Dust period	Photochemical period	Non-polluted period
HONO (ppbv)	0.57 ± 0.39	0.44 ± 0.29	0.40 ± 0.34
HONO/NO$_2$	0.07 ± 0.04	0.10 ± 0.13	0.10 ± 0.12
NO (ppbv)	1.8 ± 1.8	1.2 ± 1.4	1.8 ± 2.0
NO$_2$ (ppbv)	9.8 ± 5.0	7.1 ± 4.4	7.1 ± 4.6
O$_3$ (ppbv)	58.0 ± 10.8	78.8 ± 17.3	54.9 ± 11.7
CO (ppbv)	371.8 ± 151.9	353.8 ± 117.5	277.6 ± 98.0
SO$_2$ (ppbv)	1.6 ± 1.3	1.7 ± 0.8	0.7 ± 0.6
PM$_{2.5}$ ($\mu g\ m^{-3}$)	45.4 ± 32.3	25.0 ± 17.4	17.2 ± 12.6
PM$_{10}$ ($\mu g\ m^{-3}$)	235.3 ± 200.8	68.0 ± 47.2	32.8 ± 21.8
Sa ($m^2\ m^{-3}$)	$1.28 \times 10^{-3} \pm 8.41 \times 10^{-4}$	$6.81 \times 10^{-4} \pm 4.73 \times 10^{-4}$	$5.58 \times 10^{-4} \pm 4.22 \times 10^{-4}$
pNO$_3^-$ ($\mu g\ m^{-3}$)	7.0 ± 6.2	6.2 ± 5.6	3.0 ± 3.4
TEMP (°C)	19.0 ± 3.4	20.5 ± 2.7	15.1 ± 2.4
RH (%)	47.8 ± 24.7	47.4 ± 17.2	71.6 ± 27.0
WS ($m\ s^{-1}$)	0.42 ± 0.35	0.65 ± 0.33	0.38 ± 0.25
JNO$_2$ (s^{-1})	$6.6 \times 10^{-3} \pm 2.2 \times 10^{-3}$	$7.0 \times 10^{-3} \pm 2.1 \times 10^{-3}$	$4.5 \times 10^{-3} \pm 2.2 \times 10^{-3}$

841